

Propane-air explosions in an 8-m³ vessel with small vents: Dynamics of pressure and external flame-jet

Boeck L.R.*, Bauwens C.R., Dorofeev S.B.

FM Global, Research Division, Norwood, MA, USA

**Corresponding author's email: lorenz.boeck@fmglobal.com*

ABSTRACT

Confined and vented explosion tests were performed in an 8-m³ vessel with stoichiometric propane-air mixtures. Small vent areas consistent with the size of typical vessel-pipe connections were explored, ranging between 0.13 m² and 0.0079 m². These vent areas generated high reduced pressures, between 3.2 barg and 7.2 barg. Flame arrival times at the vent and the external flame shape were captured using high-speed video. Five distinct phases during the vented explosions were identified: (i) flame propagation from the point of ignition to the vent; (ii) external explosion consuming previously vented unburned mixture; (iii) short flame-jet; (iv) rapid increase in pressure and flame length up to peak explosion pressure; (v) decay of pressure and flame length. It was found that smaller vent areas result in later flame arrival at the vent, higher peak pressures, weaker external explosions, shorter flame-jets, and a smaller degree of combustion acceleration in phase (iv). A previously developed model for confined, simply-vented and pipe-vented explosions is compared against the experiments. It is shown that early pressure transients, and flame arrival times at the vent, are predicted with reasonable accuracy.

KEYWORDS: Gas explosions, venting, explosion isolation, propane.

INTRODUCTION

Explosion venting is a passive method to mitigate damage from industrial explosions by reducing the peak explosion pressure below the design strength of the protected enclosure. The pressures that develop depend on multiple parameters, such as the vent size, the number and location of vents, the vent deployment pressure, obstructions, the composition of the combustible atmosphere, ambient conditions and the ignition location [1, 4, 7, 14].

While the vast majority of previous large-scale studies have focused on vent sizes that reduce the peak explosion pressure sufficiently to protect low-strength industrial enclosures, typically below 0.5 barg, the present work explores significantly smaller vent areas and higher reduced pressures. The vent areas are consistent with typical pipe diameters of interconnected vessels, which is relevant for assessing the performance of explosion isolation systems. In this work, large-scale vented explosion experiments were performed to measure internal pressure, and acquire high-speed video of the external flame to characterize the flame time of arrival at the vent and extent of the external flame jet.

Data collected from the tests is compared against results from a physics-based model, which was developed to predict pressure transients and flame progress in confined, simply-vented and pipe-vented explosions. Ultimately, this model will be used to provide guidance on the proper selection and installation of explosion isolation systems, which provide protection by preventing flame propagation between enclosures connected by pipes. To that end, predicting flame arrival times at the pipe inlet of a primary enclosure, and along the pipe, is crucial to determining the isolation

system installation distance. The present tests are used to verify and calibrate the elements of the model which describe flame propagation inside the vessel and flame advection towards the vent.

EXPERIMENT AND DIAGNOSTICS

In this study, confined and vented tests with initially quiescent stoichiometric propane-air mixtures were performed in an 8-m³ vessel with an aspect ratio (height divided by diameter) of 1.4, shown in Fig. 1. For the vented tests, the vessel was equipped with an adapter flange which accepts orifice plates made from class 300 flanges. Orifice diameters of 400 mm, 200 mm and 100 mm were examined.

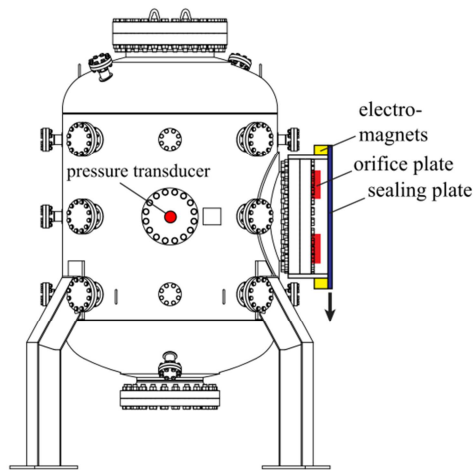


Fig. 1. Schematic of the 8-m³ explosion vessel showing orifice and sealing plates, held by electromagnets, and pressure transducer location.

A steel plate, held in place by electromagnets, was used to seal the vent during mixture preparation and was released 1 s prior to ignition. Using this method, the vent was fully open at the time of ignition, representing an ideal vent without introducing any effect of vent deployment, in contrast to other procedures using a plastic film or vent panels which significantly affect the initial outflow of the vent and the flame time of arrival at the vent.

Mixture preparation involved flushing the vessel with fresh air, adding an estimated mass of propane to reach a target concentration of 4%, generating a uniform mixture using a recirculation pump, and measuring propane concentration using infrared absorption and speed of sound analysis. The infrared absorption system comprised a 3.39 μm He-Ne laser equipped with a chopper wheel, a 50 mm long gas cell with MgF_2 windows, and two InAsSb detectors measuring laser intensity, before and after transmission through the gas cell. For speed of sound concentration measurement, a binary gas analyzer (SRS BGA244) was installed in-line with the infrared absorption system. To achieve the final target concentration, propane was incrementally added as needed while the mixture was circulated and analyzed.

For all experiments performed in this study, the mixtures were ignited by a weak electric spark (miniature spark plug with a 2 mm spark gap) at the center of the vessel.

Pressure in the vessel was measured using a piezoresistive Kistler 4260A 0-10 bara transducer located at a side flange, as indicated in Fig. 1. Two additional transducers, located at different flanges, were used to confirm that the pressure measurement location had no effect on the results.

All pressure traces presented in this work were filtered with a 200 Hz low-pass filter. High-speed video of the external flame was recorded using a Phantom Flex color camera operating at a framing rate of 500 fps.

PHYSICS-BASED MODEL

A physics-based model was recently developed to predict pressure and flame-progress as a function of time for confined explosions, simply-vented explosions and pipe-vented explosions [3]. In the present paper, selected elements of this model are compared against experiments. In particular, this study is focused on the initial flame propagation, between ignition and flame arrival at the vent. The model is described in detail in [3]; therefore, only those elements of the model which are most relevant for the present study are highlighted.

The model assumes spherical flame propagation in a spherical vessel, representative of compact enclosures, and considers the conversion of unburned mass, m_u , to burned mass, m_b , at a rate that depends on burning velocity, S , unburned gas density, ρ_u , and flame surface area, A_f ,

$$\frac{dm_u}{dt} = -\dot{m}_{v,u} - S\rho_u A_f, \quad (1)$$

$$\frac{dm_b}{dt} = -\dot{m}_{v,b} + S\rho_u A_f, \quad (2)$$

where the mass flow rates $\dot{m}_{v,u}$ and $\dot{m}_{v,b}$ represent venting of unburned and burned gas, respectively. The expansion of the burned gas due to combustion is accounted for by considering isentropic expansion of the burned gas from the constant-volume explosion pressure, p_{max} , and isentropic compression of unburned gas from its initial density, ρ_0 , and initial pressure, p_0 , to the time-dependent vessel pressure, p :

$$p = p_{max} \left(\frac{\rho_b}{\rho_0} \right)^{\gamma^*}; \quad (3)$$

$$\rho_u = \rho_0 \left(\frac{p}{p_0} \right)^{1/\gamma_u}. \quad (4)$$

The effective exponent for expansion of burned products is given by

$$\gamma^* = \frac{\log(p_0/p_{max})}{\log(1/\sigma_0)}, \quad (5)$$

using the expansion ratio, σ_0 , at initial pressure, p_0 . The burning velocity, S , is calculated from the laminar burning velocity at initial pressure and temperature, $S_{L,0}$, taking into account the effects of pressure, p , and temperature of the unburned gas, T_u , over the course of the explosion,

$$S_L = S_{L,0} \left(\frac{T_u}{T_0} \right)^a \left(\frac{p}{p_0} \right)^b, \quad (6)$$

as well as the effect of flame instabilities using a power-law relationship,

$$S = S_L \left(\frac{r_f}{r_{crit}} \right)^\beta, \quad (7)$$

which applies for flame radii, r_f , greater than the critical radius for the onset of instabilities, r_{crit} . Equations (1)-(7) are solved to predict confined explosions. For vented explosions, the flow rate through the vent is calculated for sub-sonic flow as given in [1],

$$u_v = \pm C_d \sqrt{2 \left(\frac{\gamma_v}{\gamma_v - 1} \right) \left(\frac{p}{\rho_v} \right) \left[1 - \left(\frac{p_e}{p} \right)^{(\gamma_v - 1)/\gamma_v} \right]}. \quad (8)$$

Here, u_v is the area-averaged flow velocity in the vent, C_d is the discharge coefficient, ρ_v and γ_v are the density and isentropic exponent of vented gas, respectively, and p_e is the pressure outside the vent. Unburned mixture is vented before the flame arrives at the vent, therefore $\rho_v = \rho_u$ and $\gamma_v = \gamma_u$. After the flame has arrived at the vent, both unburned and burned gases are vented simultaneously. The fraction of vented unburned gas, X_v , as a function of flame volume, V_f , and vessel volume, V , is approximated as

$$X_v = (V - V_f)/V. \quad (9)$$

Density and isentropic exponent of vented gas are determined from

$$\rho_v = X_v \rho_u + (1 - X_v) \rho_b, \quad (10)$$

$$\gamma_v = \frac{X_v c_{p,u} + (1 - X_v) c_{p,b}}{X_v c_{v,u} + (1 - X_v) c_{v,b}}, \quad (11)$$

where $c_{p,u}$ and $c_{p,b}$ are the specific heat capacities of unburned and burned gas, respectively. The total vented mass flow rate for a vent area A_v becomes

$$\dot{m}_v = A_v u_v \rho_v (p_e/p)^{1/\gamma_v}. \quad (12)$$

Since the flame is advected toward the vent as soon as pressure in the vessel increases and flow through the vent occurs, a model is needed to determine the advection velocity of the flame edge closest to the vent to correctly capture the flame arrival time at the vent. For explosions with small vent areas or connected pipes, we assume that the flame geometry can be described as a sphere with a conical section extending toward the vent. The instantaneous flame advection velocity due to unburned gas venting depends primarily on the instantaneous pressure difference between vessel and surroundings, the vent size, and the distance between the vent and leading flame-edge. In the present simplified model, streamlines for gas flowing toward the vent are assumed to be oriented perpendicular to a hemispherical surface centered at a virtual origin near the vent. The flow velocity at the location of the leading flame tip, u_x , is expressed implicitly, and a calibration constant, k_v , is used to account for the simplifications made in describing flame geometry and flow field:

$$\dot{m}_v = 2u_x x_f^{*2} \pi \rho_v k_v \left(1 - \frac{u_x^2}{2 \frac{\gamma_v p}{\gamma_v - 1} \rho_v}\right)^{1/(\gamma_v - 1)}. \quad (13)$$

The flame tip location is written with respect to the virtual origin,

$$x_f^* = (R - x_f) + R_v/\sqrt{2}, \quad (14)$$

where R is the vessel radius, x_f is the location of the leading flame tip measured from the ignition location, and R_v is the vent radius.

The external pressure outside the vent, p_e , is equal to atmospheric pressure before flame arrival at the vent. As the flame arrives at the vent, the cloud of previously vented unburned mixture is ignited and an external explosion occurs, which temporarily increases p_e . A model proposed by Strehlow [12], based on acoustic theory, is used to obtain the pressure caused by the external explosion,

$$\frac{p_e}{p_0} - 1 = \frac{\gamma(\sigma - 1)}{4\pi a_0^2 R_e} \frac{d}{dt} (S_e A_{f,e}), \quad (15)$$

where a_0 is the speed of sound in the external cloud, R_e is the external cloud radius, and S_e and $A_{f,e}$ are the burning velocity and flame surface area within the external cloud, respectively. Further relations needed to solve this equation are given in [3]. After the vented unburned mixture is consumed, external pressure again equals atmospheric pressure.

To compare the model results with the experiments, the model parameters given in the Appendix, Table 5, were used.

EXPERIMENTAL RESULTS AND MODEL COMPARISON

This section presents experimental results from confined and vented tests, and compares the data against model predictions. For each configuration, three repeat tests were performed at nominally identical conditions. The results from vented tests with a 400 mm orifice will be used to describe the general behavior observed throughout the tests. These are discussed in more detail than the smaller orifice diameter tests, which will be used for model comparison. For all of the results, time $t = 0$ s refers to the time of ignition. A summary of all tests is given in the Appendix.

Confined tests

Figure 2 shows experimental pressure traces (solid black lines) and model predictions (dashed red line) for confined explosions.

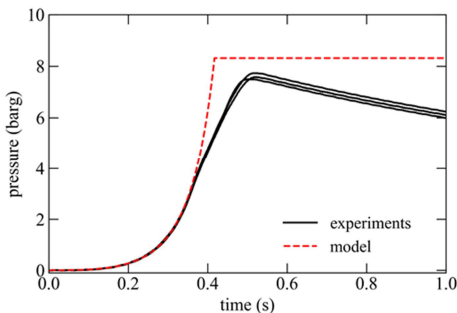


Fig. 2. Pressure traces from confined tests.

Experiments (black solid lines) and model prediction (red dashed line).

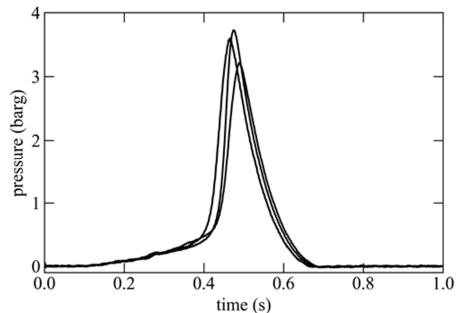


Fig. 3. Pressure traces from tests with 400-mm orifice.

Peak constant volume explosion pressures of 7.4 barg to 7.6 barg are reached approximately 0.5 s after ignition with a maximum rate of pressure rise of 41-44 bar/s, as determined from the pressure histories using an 80 Hz low-pass filter. The model prediction shows good agreement with the experiments for pressures below 4 barg. At higher pressures, corresponding to larger flame sizes, measured pressures are lower than the model predictions due to heat loss in the experiment, which is not taken into account in the model. It should be noted, that while accounting for heat loss in the model may better approximate specific experiments, additional uncertainty is introduced, which may lead to situations where model predictions are not conservative. To avoid the potential for under-conservative results, heat loss is not accounted for in this model. Previous comparisons against tests in 2.4-m³ and 25-m³ vessels showed similarly favorable comparisons [3], which demonstrates that the model is able to predict the effect of scale and reasonable burning rates for confined large-scale explosions.

Vented tests: 400 mm orifice

Figure 3 shows experimental pressure traces for vented explosions with a 400 mm orifice. Peak pressures measured in these three tests range between 3.2 barg and 3.7 barg, attained between 0.46 s and 0.49 s after ignition. Despite venting, the maximum rates of pressure rise are higher than the values of the confined tests and vary significantly between tests, 75-116 bar/s.

Figure 4 shows images of the external flame-jet at selected times. Image #1 shows flame arrival at the vent at $t = 161$ ms after ignition. The following images, #2-5, show the external explosion where

the previously vented unburned gas is consumed. Following the external explosion, the flame length reduces significantly, #6-8, before the flame length increases rapidly and features of an under-expanded jet become visible, #9-11. Finally, flame length decreases after burnout has occurred in the vessel.

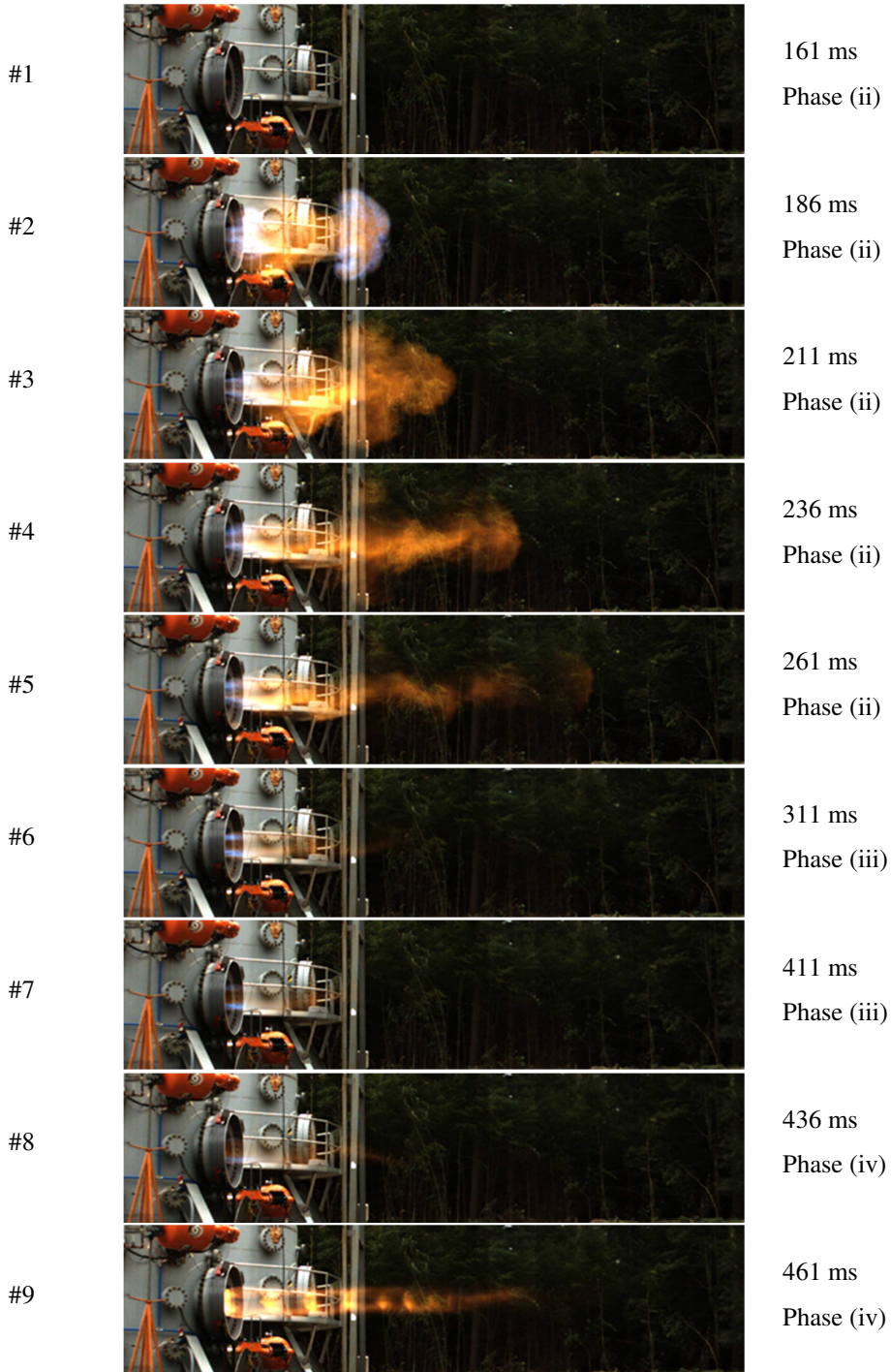




Fig. 4. Image sequence from a selected 400-mm orifice test (Vented-400-2) showing external flame.

Five phases in Fig. 4 can be identified:

- (i) flame propagation from the point of ignition to the vent, $0 \text{ ms} \leq t < 161 \text{ ms}$;
- (ii) external explosion with increasing flame length and peak flame width, $161 \text{ ms} \leq t < 267 \text{ ms}$;
- (iii) short flame-jet with gradual pressure build-up, $267 \text{ ms} \leq t < 430 \text{ ms}$;
- (iv) rapid lengthening of the flame-jet and sharp pressure increase, including a period of choked flow at the orifice, $430 \text{ ms} \leq t < 475 \text{ ms}$;
- (v) decreasing flame-jet length and pressure, $t \geq 475 \text{ ms}$. The end of burned-gas venting can be estimated from the pressure trace at about 680 ms.

Figure 5 shows simultaneous measurements of the flame length (horizontal distance between vent and leading flame-edge) and the maximum flame width (maximum vertical distance between lower and upper flame-edge), obtained from high-speed video, using background-subtraction and thresholding, plotted with the pressure trace of this test.

The peak pressure predicted by the model for the present case is about 1 barg, clearly underestimating the experimentally observed peak pressure. This discrepancy, as well as the high rate of pressure rise during phase (iv), higher than the peak rate of pressure rise in the confined explosions, indicates intense acceleration of burning rates at this time. It is known from previous work [1] that flame-acoustic interactions close to burnout can strongly accelerate combustion, an effect that is not included in the present model. Shock oscillations of the underexpanded jet [9,10] may contribute to flame acceleration at late times during phase (iv). Future work is needed to explore the effect of venting on flame-acoustic interactions.

The present model is designed to predict the early explosion process, which is relevant for explosion isolation system design. Figure 6 provides a comparison between experiments and model for phases (i) and (ii), including flame propagation toward the vent, and the external explosion. The parameter

which calibrates the flame advection model in Eq. (13), is determined based on all present tests as $k_v = 0.35$. The model predicts the pressure history of phases (i) and (ii) with a reasonable accuracy. The end of the external explosion is predicted at $t = 248$ ms, which is between the time of maximum flame width, $t = 240$ ms, and the time of maximum flame length, $t = 267$ ms. At the beginning of phase (iii), pressure in the experiment increases at a faster rate than in the model, indicating the onset of flame-acoustic interactions leading to flame acceleration.

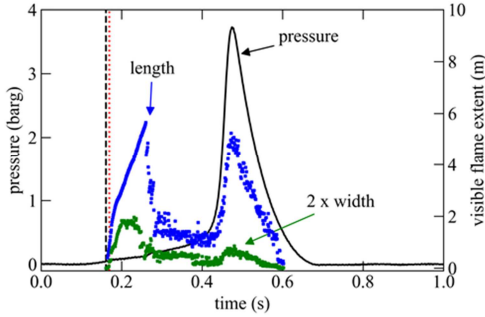


Fig. 5. Pressure trace and visible flame extent (length and width) for a selected 400-mm orifice test (Vented-400-2).

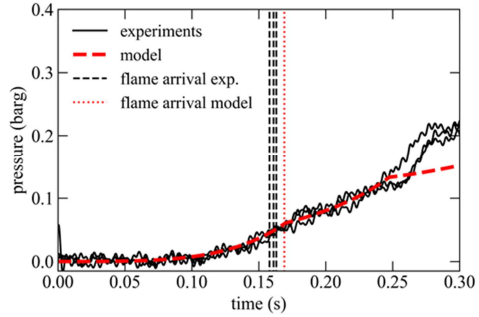


Fig. 6. Pressure histories during phases (i) and (ii) for the 400-mm orifice. Experiments (black lines) and model prediction (red lines).

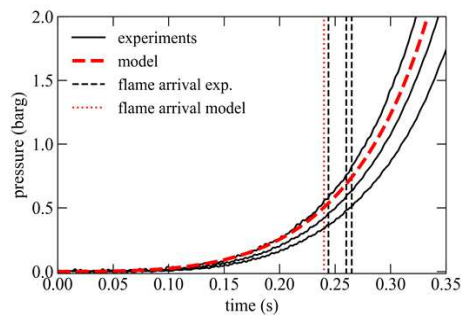
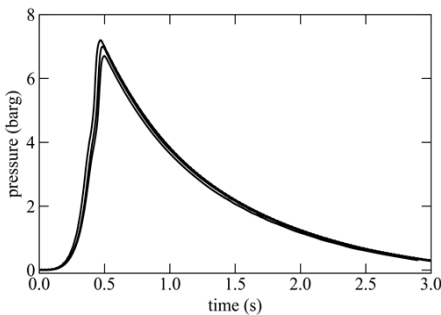
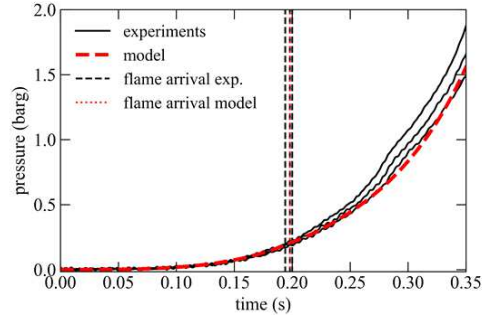
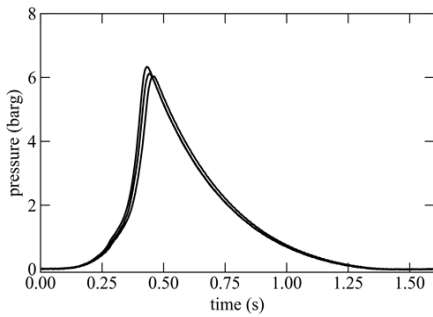


Fig. 7. Pressure traces from tests with 200-mm orifice (top) and 100-mm orifice (bottom). Experiments (black solid lines) and model predictions (red dashed lines).

Vented tests: 200 mm and 100 mm orifices

Pressure traces from experiments with the 200 mm and 100 mm orifices are shown in Fig. 7. Peak pressure ranges between 6.0 barg and 6.3 barg for the 200 mm orifice, and between 6.7 barg and 7.2 barg for the 100 mm orifice. Maximum rates of pressure rise are 77-90 bar/s and 74-92 bar/s for

the 200 mm and 100 mm orifice, respectively. The initial pressure increases during phase (i), as well as flame arrival times, are captured well by the model for both cases, see Fig. 7, right panels.

Similar to the 400 mm orifice, the flame length histories, Fig. 8, show two peaks, where the first peak corresponds to the external explosion, and the second peak coincides with the time of maximum pressure. The pressure increase is rather continuous between phase (iii) and phase (iv), in contrast to a sharp increase during phase (iv) for the 400 mm orifice, indicating that the acceleration of combustion during phase (iv) is weaker for the 200 mm and 100 mm orifices than for the 400 mm orifice. The maximum external flame length decreases with decreasing orifice diameter.

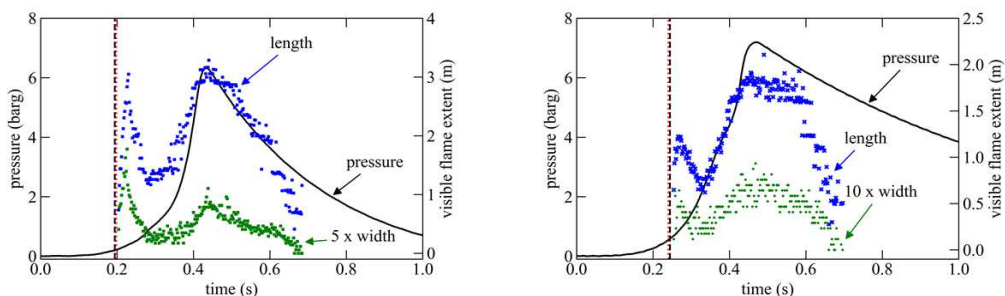


Fig. 8. Pressure trace and visible flame extent (length and width) for a 200-mm orifice test (Vented-200-1, left) and a 100-mm orifice test (Vented-100-1, right).

CONCLUSIONS

In this study, confined and vented explosion tests in an 8-m³ vessel with stoichiometric propane-air mixtures were performed, with a focus on small vent areas. The goals were to capture the pressure and flame dynamics and to provide data for the calibration and verification of a model developed to predict confined, simply-vented and pipe-vented explosions to ultimately support the development of guidelines for the proper selection and installation of explosion isolation systems.

Two results should be highlighted:

- The calibrated model was able to capture pressure traces for confined explosions, as well as early pressure traces for vented explosions. Flame arrival at the vent was predicted with an accuracy of $\pm 10\%$, which shows that the model can capture the increase in flame arrival time at the vent with decreasing vent size. The model under-estimated the overall peak pressure for the largest orifice. This is due to secondary acceleration of combustion near burnout, an effect that is currently not considered in the model, as it is not a factor that would affect the installation distance of explosion isolation systems.
- For the largest orifice tested, strong secondary acceleration of combustion inside the vessel occurred after the external explosion, which led to a high second pressure peak and long flame-jet. This acceleration effect was significantly weaker for the smaller orifice cases tested. Further study is needed to investigate whether this acceleration is due to acoustics-flame interactions as observed in previous work, and to determine the effect of venting on such interactions.

Future work will include experiments with different mixtures and ignition locations. For further calibration and verification of the model, tests with pipes attached to the vessel will be performed.

REFERENCES

- [1] C.R. Bauwens, J. Chaffee and S.B. Dorofeev, Effect of Ignition Location, Vent Size and Obstacles on Vented Explosion Overpressure in Propane-Air Mixtures, *Combust. Sci. Techn.* 182 (2010) 1915-1932.
- [2] C.R. Bauwens, J.M. Berghthorson, S.B. Dorofeev, Experimental study of spherical-flame acceleration mechanisms in large-scale propane-air flames, *Proc. Combust. Inst.* 35 (2015) 2059-2066.
- [3] L.R. Boeck, C.R. Bauwens, S.B. Dorofeev, A physics-based model for explosions in vented vessel-pipe systems. 12th ISHPMIE, Kansas City, MO, USA (2018).
- [4] M.G. Cooper, M. Fairweather and J.P. Tite, On the Mechanisms of Pressure Generation in Vented Explosions, *Combust. Flame* 65 (1986) 1-14.
- [5] D.G. Goodwin, H.K. Moffat, R.L. Speth, Cantera: An object-oriented software toolkit for chemical kinetics, thermodynamics, and transport processes, version 2.3 (2017).
- [6] M. Goswami, S.C.R. Derks, K. Coumans, W.J. Slikker, M.H. de Andrade Oliveira, R.J. Bastiaans, C.C.M. Luijten, L.P.H. de Goey, A.A. Konnov, The effect of elevated pressures on the laminar burning velocity of methane-air mixtures, *Combust. Flame* 160 (2013) 1627-1635.
- [7] A. J. Harrison, J. A. Eyre, External explosions as a result of explosion venting, *Combust. Sci. Techn.* 52 (1987) 91-106.
- [8] M. Metghalchi, J.C. Keck, Laminar burning velocity of propane-air mixtures at high temperature and pressure, *Combust. Flame* 38 (1980) 143-154.
- [9] J. Panda, Shock oscillation in underexpanded screeching jets, *J. Fluid Mech.* 363 (1998) 173-198.
- [10] A. Powell, On the mechanism of choked jet noise, *Proc. Phys. Soc. B* 66 (1953) 1039.
- [11] G.P. Smith, D.M. Golden, M. Frenklach, N.W. Moriarty, B. Eiteneer, M. Goldenberg, T. Bowman, R.K. Hanson, S. Song, W.C. Gardiner Jr., V.V. Lissianski, Z. Qin, GRI-Mech 3.0. http://www.me.berkeley.edu/gri_mech/ (accessed 05 September 2018).
- [12] R.A. Strehlow, The blast wave from deflagrative explosions, an acoustic approach. Tech. rep., University of Illinois, 1979.
- [13] C.M. Vagelopoulos, F.N. Egolfopoulos, C.K. Law, Further considerations on the determination of laminar flame speeds with the counterflow twin-flame technique, *Proc. Combust. Inst.* 25 (1994) 1341-1347.
- [14] R.G. Zalosh, Gas Explosion Tests in Room-Size Vented Enclosures, In: Proceedings of the 13th Loss Prevention Symposium, Houston, 1979, pp. 98-108.

APPENDIX

Table 1. Summary of confined tests

| Test number | $X_{C_3H_8}$ (%) \pm 0.05 | p_{max} (barg) | $(dp/dt)_{max}$ (bar/s) |
|-------------|--------------------------------|---------------------|----------------------------|
| Confined-1 | 4.05 | 7.4 | 41 |
| Confined-2 | 4.07 | 7.6 | 44 |
| Confined-3 | 4.06 | 7.5 | 43 |

Table 2. Summary of vented tests with 400 mm orifice

| Test number | $X_{C_3H_8}$ (%) ± 0.05 | p_{max} (barg) | $(dp/dt)_{max}$ (bar/s) | Flame arrival test (ms) | Flame arrival model (ms) |
|--------------|--------------------------------|---------------------|----------------------------|----------------------------|-----------------------------|
| Vented-400-1 | 4.11 | 3.6 | 80 | 158 | |
| Vented-400-2 | 4.15 | 3.7 | 116 | 161 | 169 |
| Vented-400-3 | 4.07 | 3.2 | 75 | 163 | |

Table 3. Summary of vented tests with 200 mm orifice

| Test number | $X_{C_3H_8}$ (%) ± 0.05 | p_{max} (barg) | $(dp/dt)_{max}$ (bar/s) | Flame arrival test (ms) | Flame arrival model (ms) |
|--------------|--------------------------------|---------------------|----------------------------|----------------------------|-----------------------------|
| Vented-200-1 | 4.09 | 6.3 | 90 | 194 | |
| Vented-200-2 | 4.06 | 6.0 | 77 | 200 | 198 |
| Vented-200-3 | 4.10 | 6.1 | 81 | 198 | |

Table 4. Summary of vented tests with 100 mm orifice

| Test number | $X_{C_3H_8}$ (%) ± 0.05 | p_{max} (barg) | $(dp/dt)_{max}$ (bar/s) | Flame arrival test (ms) | Flame arrival model (ms) |
|--------------|--------------------------------|---------------------|----------------------------|----------------------------|-----------------------------|
| Vented-100-1 | 4.09 | 7.2 | 92 | 244 | |
| Vented-100-2 | 4.13 | 6.9 | 76 | 260 | 240 |
| Vented-100-3 | 4.12 | 6.7 | 74 | 265 | |

Table 5. Summary of model parameters

| $S_{L,0}$ (m/s) | σ_0 (-) | p_{max} (barg) | γ_u (-) | γ_b (-) | a (-) | b (-) | r_{crit} (m) | β (-) | C_d (-) | k_v (-) | k_e (-) |
|--------------------|-------------------|---------------------|-------------------|-------------------|-------------|--------------|-------------------|----------------|--------------|--------------|--------------|
| 0.40 [13] | 8.0 [5, 11] | 8.4 [5, 11] | 1.37 [5, 11] | 1.25 [5, 11] | 2.13 [8] | -0.17 [8] | 0.20 [2] | 0.20 [2] | 0.70 | 0.35 | 0.35 |